Vector field path following and obstacle avoidance singularity mitigation via look-ahead flight envelope

First A. Author* and Second B. Author Jr.†
Business or Academic Affiliation 1, City, State, Zip Code

Unmanned Aerial Vehicles conventionally navigate by following a series of pre-planned waypoints that may have to be re-planned when flying in a dynamic environment or encountering previously unknown obstacles. Waypoints are generally planned off-line and relayed to the UAV, taking up time and autopilot communication resources. Attractive path following and repulsive obstacle avoidance vector fields have been summed together to produce UAV guidance that follows pre-planned paths and avoids obstacles without the need to re-plan. Summing attractive and repulsive vector fields may produce small regions of null guidance, called singularities, which could potentially lead to trap situations. An investigation into singularity mitigation by vector field weight parameterization is presented.

I. Nomenclature

UAV = Unmanned Aerial Vehicle
VF = Vector Field
VFF = Virtual Force Field
LVF = Lyapunov Vector Field
GVF = Goncalves Vector Field

II. Introduction

Unmanned Aerial Vehicles are pilotless aircraft used by military, police, and civilian communities for tasks such as reconnaissance, damage assessment, surveying, and target tracking [1, 2]. Tasks can be performed by a single UAV or cooperate with a team of other air, ground, or marine vehicles [3–5]. UAVs can be programmed to loiter around an area of interest or follow a prescribed path, such as a road or tree line, where data can be collected for extended periods of time. When collecting data it is important to stay as close to a prescribed path as possible to maximize sensor coverage of the area while avoiding collisions.Obstacle free and flyable paths are typically pre-planned and generated off-line at a dedicated ground station using a path planner. Many methods can be used for generating paths, however the process is generally executed in two steps consisting of optimization and refinement. Optimization builds shortest path taking in constraints such as obstacles and mission objectives. The optimized path is then refined to meet a vehicles dynamic constraints, such as turn rate and velocity. UAVs using a line-of-sight guidance are sent a series of waypoints that lie along the pre-planned path over radio. The autopilot's guidance system directs the UAV to turn the crafts heading towards the current active waypoint, traveling in circular arcs and straight paths. Curved sections of the refined path may require a dense spacing of waypoints to ensure the UAV tracks the refined path accurately. An example of a UAV following a series of waypoints that lie along a prescribed path is shown in Figure ().

*Insert Job Title, Department Name, Address/Mail Stop, and AIAA Member Grade (if any) for first author.
†Insert Job Title, Department Name, Address/Mail Stop, and AIAA Member Grade (if any) for second author.

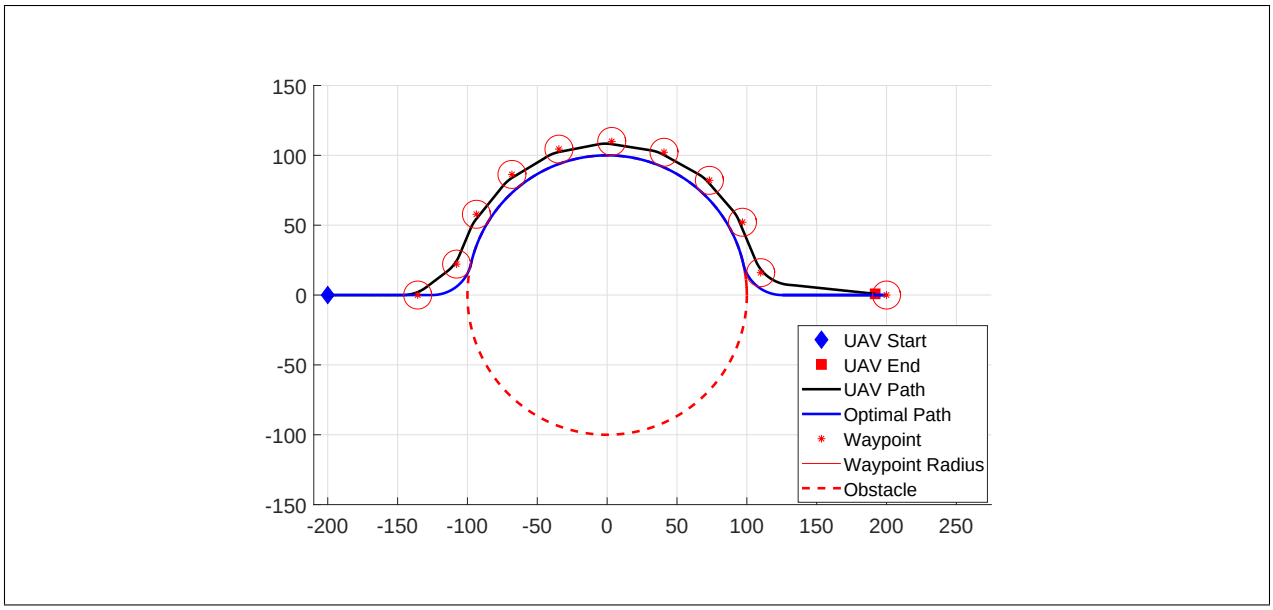

Fig. 2

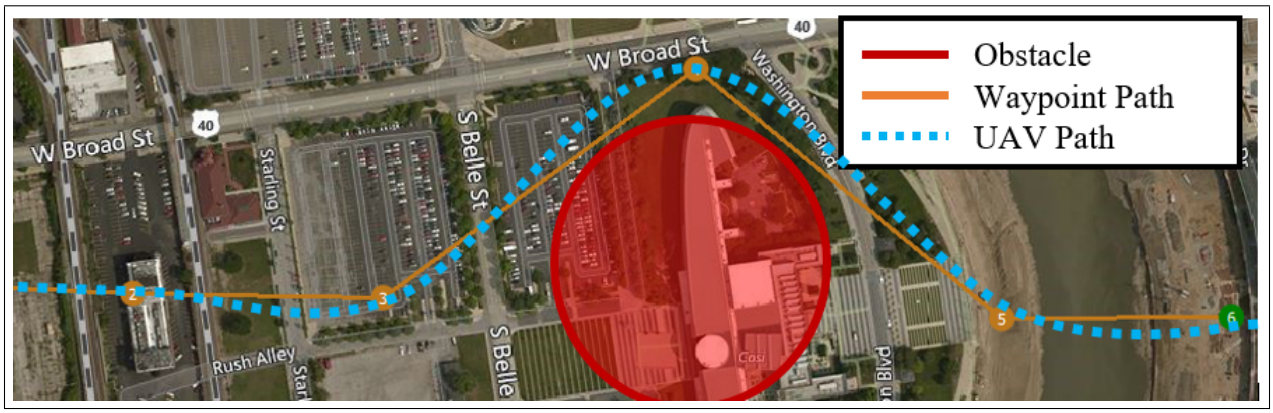

Fig. 1 UAV path from waypoint guidance

During waypoint navigation the UAV may encounter obstacles or environmental changes that would require a new obstacle free series of waypoints to be generated. UAVs that rely on off-board path planning would relay the updated environment information to the ground where a new optimized, refined, and obstacle free path would be re-planned. Waypoints would be constructed along the updated path and relayed back to the UAV. For highly uncertain or dynamic environments, path planning may have to occur frequently which may be impossible if the UAV is flying beyond LOS or needs to maintain radio silence. In the event communication is possible, the latency of waypoint updates may not be frequent enough and the UAV may fail to avoid obstacles all together.

III. Optimal Path

$$y = \frac{u}{\dot{theta}} \tag{1}$$

$$X = obstX - \sqrt{(turnR - obstR)^2 - (y - obstY)^2} \tag{2}$$

$$\Theta = \sin^{-1}\left(\frac{y - obstY}{obstR + turnR}\right) \tag{3}$$

$$\beta = \left[\frac{3\pi}{2}, \pi - \Theta\right] \tag{4}$$

$$\gamma = \left[\pi - \Theta, \Theta\right] \tag{5}$$

$$\zeta = \left[\pi + \Theta, \frac{30pi}{2}\right] \tag{6}$$

$$x = \begin{cases} 0 & X + turnR * cos(beta) \\ \frac{100-x}{100} & obstX + obstR * cos(gamma) \\ 0 & -X + turnR * cos(zeta) \end{cases} \tag{7}$$

A. Potential Field

Obstacle free paths in static and dynamic environments have been generated with the potential field method, which models a robot's workspace as a gradient of artificial attractive and repulsive forces [7]. Potential field combines path planning, trajectory planning, and control into a single system [8]. Paths can be generated by placing a point mass at an initially high potential and allowing it to descend a gradient until the point reaches the goal, located at a global minimum potential. Obstacles provide a limited repulsive force, pushing the mass away from the obstacle.

A histogram based potential field method can be found in [9–11] which allowed for real time goal seeking with obstacle avoidance. Sensors on-board a ground robot located at (x_0, y_0) detect obstacles within a pre-defined window containing a fixed number of cells. Cells containing an obstacle provide a repulsive force $\overrightarrow{F_{i,j}}$ opposite in direction to the line-of-sight from vehicle to cell location (x_i, y_j), where (i, j) represents the cell index, F_{cr} is a constant repulsive force, W the vehicle's width, $C_{i,j}$ a cell's certainty, and $d_{i,j}$ the distance to the center of the cell with respect to robots center.

$$\overrightarrow{F_{i,j}} = \frac{F_{cr} W^n C_{i,j}}{d_{i,j}^n} \left(\frac{x_i - x_0}{d_{i,j}} \hat{x} + \frac{y_i - y_0}{d_{i,j}} \hat{y} \right) \tag{8}$$

The total repulsive force exerted on the robot is determined by summing the active cells, shown in Equation 9

$$\overrightarrow{F_r} = \sum_{i,j} \overrightarrow{F_{i,j}} \tag{9}$$

The robot is attracted to the goal by force $\overrightarrow{F_t}$ with constant magnitude F_{ct} and along the LOS from robot center to goal, located at (x_t, y_t) and a distance d_t, shown in Equation 10

$$\overrightarrow{F_t} = F_{ct} \left(\frac{x_t - x_0}{d_t} \hat{x} + \frac{y_t - y_0}{d_t} \hat{y} \right) \tag{10}$$

Summing together attractive and repulsive forces produce a vector that can be used for heading guidance, shown in Equation 11.

$$\overrightarrow{R} = \overrightarrow{F_r} + \overrightarrow{F_t} \tag{11}$$

Major drawbacks to potential field were identified in [11] consisting of local minimum and oscillations in corridors. The local minimum problem occurs when closely spaced obstacle's potential combine to produce a well on the descent gradient where a pre-mature stable point is found. Proposed solutions to local minimum include object clustering and virtual waypoint method [12], virtual escaping route [13], and use of navigation functions [14]. Oscillations in potential field were studied in [15] and [16].

In addition to local minimum and oscillations, potential field may converge to a singular point which is not possible for fixed wing aircraft since it must maintain a minimum forward velocity to remain airborne. Similar to conventional waypoint guidance, the active goal point would change as a function of proximity. Simulating a UAV using VFF as guidance for a Dubins vehicle was performed and is shown in Figure 3, where a single obstacle cell located at the origin. The UAV initially travels directly toward the goal located at $(50, 0)$ until the obstacle is encountered, at which point a repulsive force is applied. The UAV avoids the obstacle, however significantly deviates and fails to get back on the path

between waypoints. For certain applications it may be benefitial to follow explicit paths for tasks such as data collection on a roadway or searching a tree line.

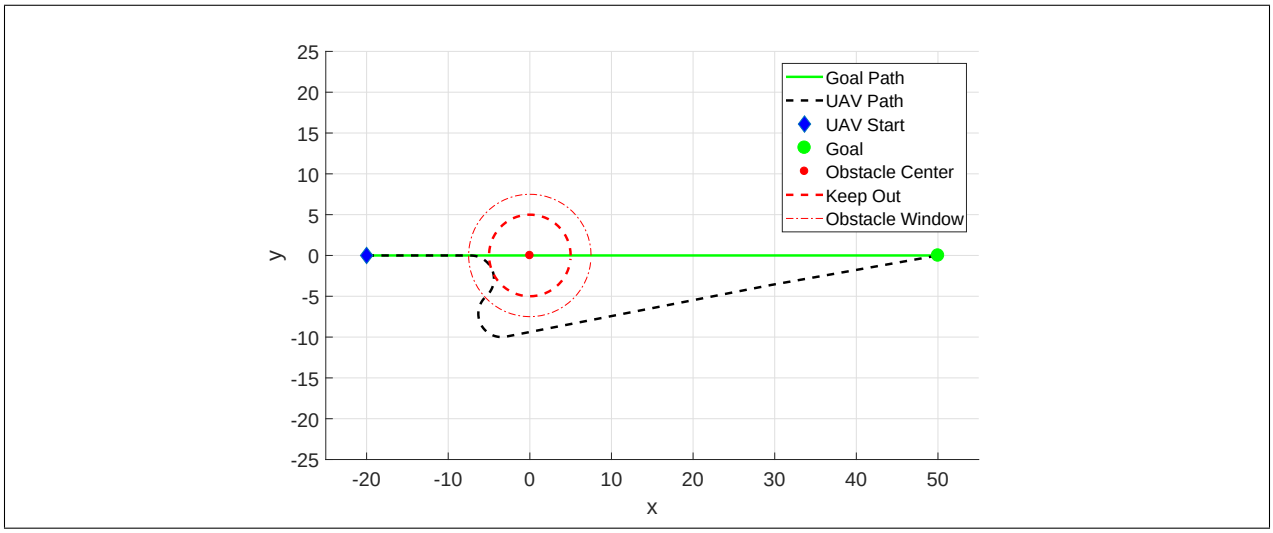

Fig. 3 Dubins vehicle encountering an obstacle while navigating to a waypoint

Following an explicit path to collect data or follow a ground target can be accomplished with vector fields, which produce a heading guidance that asymptotically converges and circulates a path. A comparison between vector field and waypoint guidance techniques was presented in [17] where each method was evaluated based on its complexity, robustness, and accuracy. The vector field model produced guidance that was both robust to external wind disturbances while maintaining a low cross track error. The two most prominent methods for generating vector fields in literature consist of the Lyapunov [18–23] and Goncalves [24–27] method. Lyapunov vector fields for converging and following straight and circular paths were described in [18].

Straight and circular path vector fields can be selectively activated throughout flight to form more complex paths, shown in [18–20, 28]. Lyapunov vector field for curved path following was presented in [23] which may allow for more complex paths and eliminates the need to switch between vector fields.

B. GVF

The Gonvalves Vector Field (GVF) method produces a similar field, however has several advantages over LVFs. GVF produces an n-dimensional vector field that converges and circulates to both static and time varying paths. Additionally, convergence, circulation, and time-varying terms that make up the GVF are decoupled from each other allowing for easy weighting of the total field. GVFs converge and circulate at the intersection, or level set, of $n-1$ dimensional implicit surfaces ($\alpha_i : \mathbb{R}^n \rightarrow \mathbb{R} | i = 1, ..., n-1$). The integral lines of the field are guaranteed to converge and circulate the level set when two conditions are met: 1) the implicit surface functions are positive definite and 2) have bounded derivatives.

The total vector field $\overrightarrow{V}$ is calculated by:

$$\overrightarrow{V} = G\nabla V + H \wedge_{i=1}^{n-1} \nabla\alpha_i - LM(\alpha)^{-1}a(\alpha) \tag{12}$$

or in component form:

$$\overrightarrow{V} = G\overrightarrow{V}_{conv} + H\overrightarrow{V}_{circ} + L\overrightarrow{V}_{tv} \tag{13}$$

where $\overrightarrow{V}_{conv}$ produces vectors perpendicular to the path, $\overrightarrow{V}_{circ}$ produces vectors parallel to the path, and $\overrightarrow{V}_{tv}$ is a feed-forward term that produces vectors accounting for a time varying path.

Convergence is calculated by:

$$\vec{V}_{conv} = \nabla V \tag{14}$$

where scalar G is multiplied by the gradient of the definite potential function V:

$$V = -\sqrt{{\alpha_1}^2 + {\alpha_2}^2} \tag{15}$$

$$\nabla V = \begin{bmatrix} \frac{dV}{dx} \\ \frac{dV}{dy} \\ \frac{dV}{dz} \end{bmatrix} \tag{16}$$

Circulation is calculated by taking the wedge product of the gradients of the surface functions:

$$\vec{V}_{circ} = \wedge_{i=1}^{n-1} \nabla \alpha_i \tag{17}$$

In the case of $(n = 3)$ the wedge product simplifies as the cross product:

$$\vec{V}_{circ} = \nabla \alpha_1 \times \nabla \alpha_2 \tag{18}$$

The feed-forward time-varying component is calculated by:

$$\vec{V}_{tv} = M^{-1} a \tag{19}$$

where,

$$M = \begin{bmatrix} \nabla \alpha_1^T \\ \nabla \alpha_2^T \\ (\nabla \alpha_1 \times \nabla \alpha_2)^T \end{bmatrix} \tag{20}$$

$$a = \begin{bmatrix} \frac{\partial \alpha_1}{\partial t} & \frac{\partial \alpha_2}{\partial t} & 0 \end{bmatrix}^T \tag{21}$$

Intersecting two flat planes $(\alpha_1 = z, \alpha_2 = x)$ produces a GVF that converges and circulates a straight path, shown in Figure 5.

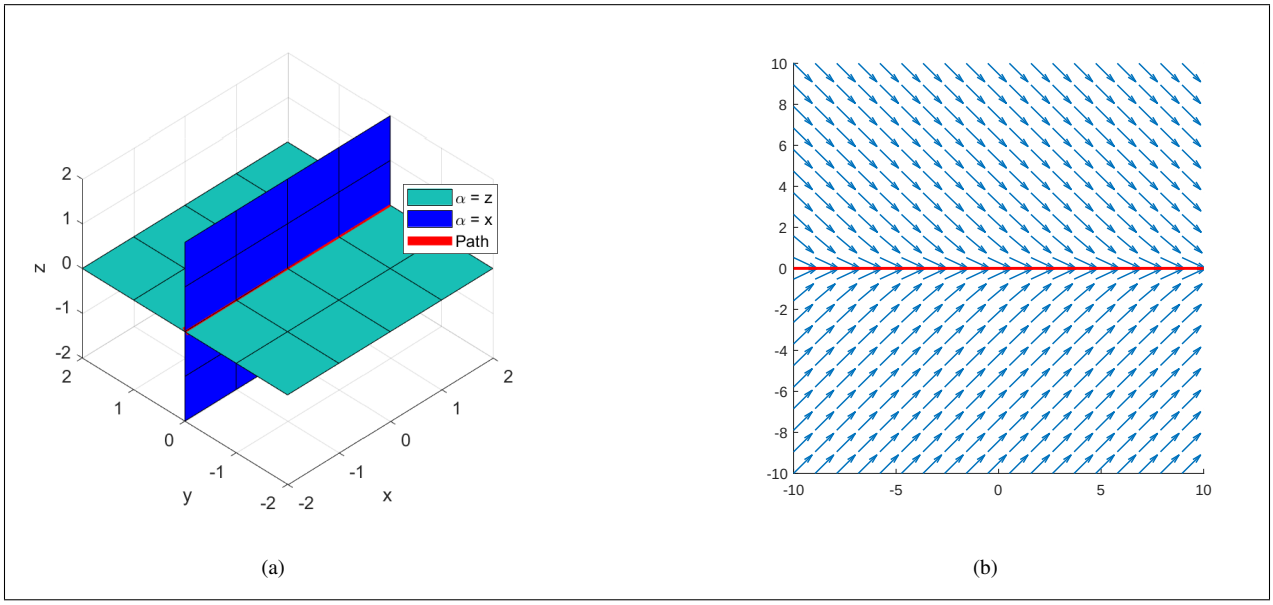

Fig. 4 GVF converging and circulating straight path

A GVF for converging and circulating a circular path can be produced by intersecting a plane and a cylinder $(\alpha_1 = z, \alpha_2 = x^2 + y^2 - r^2)$.

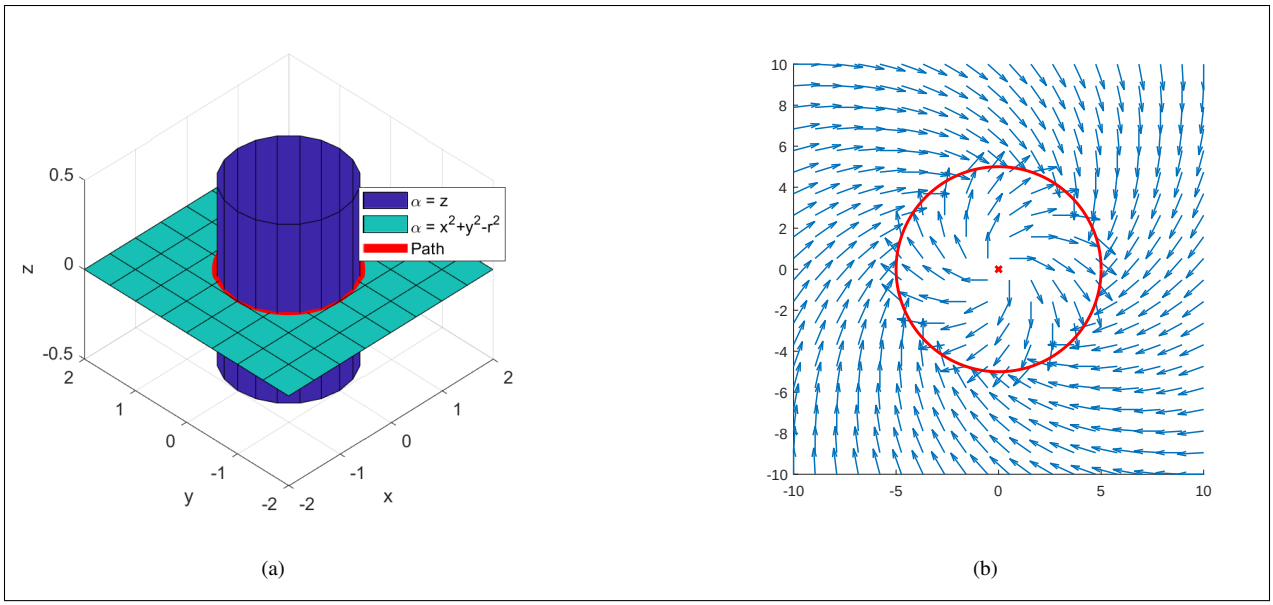

Fig. 5 GVF converging and circulating circular path

GVF was compared against LVP in a standoff tracking scenario in [Wilhelm] where a fixed wing UAV was tasked with with loitering around a moving ground target while avoiding static obstacles. A circular time-varying attractive vector field was attached to a moving ground target. Static circular repulsive vector fields centered at the obstacles and weighted by hyperbolic tangent decay functions were summed with the attractive circular field to produce a target loitering and obstacle avoidance guidance. The performance of Lyapunov [21] and gradient vector field [24–26] were compared for their cross track error with respect to the loiter circle. Gradient vector field had favorable performance due to compensation for a time-varying vector field. The gradient vector field technique also has the benefit of decoupled weighting parameters for convergence, circulation, and time-varying terms, allowing for easy modification of field behavior.

Decay functions for avoidance fields using GVF were investigated in [Zhu] for obstacles present on a straight path. When summing attractive and repulsive vector fields there is the possibility of guidance singularities, where magnitude and direction are equal and opposite. The presence of singularities were not addressed in [Wilhelm] and [Zhu], mentioned briefly in [18] and observed in [29]. For fixed wing UAVs the lack of guidance may prevent the UAV from avoiding an obstacle, while multi-rotor UAVs may end up in a trap situation. Singularities may be present at any location where a goal field and obstacle field are of equal strength.

C. Dubins Vehicle

Dubin's vehicle's position $\overrightarrow{X}$ at time t is calculated from the integral of the velocity vector $\overrightarrow{U}$. The vehicle has a constant velocity magnitude u_{uav} at a heading θ. The rate at which θ changes with respect to time is based on limitations of the craft itself.

$$\overrightarrow{U}(t) = u_{uav} \begin{bmatrix} cos(\theta(t)) \\ sin(\theta(t)) \end{bmatrix} \tag{22}$$

$$\overrightarrow{X}(t) = \overrightarrow{U}dt + \overrightarrow{X}(t-1) \tag{23}$$

$$\dot{\theta} \leq 20deg/s \tag{24}$$

IV. methods

Overview of methods
Construction of guidance for desired path
Construction of avoidance guidance
Path following and obstacle avoidance guidance
Singularity detection
Selection of vf parameters for optimized obstacle avoidance

A. Path Following with GVF

Path following guidance for a planar UAV at position (x, y) for a time invariant line is achieved by summing together convergence $\overrightarrow{V}_{conv}$ and circulation $\overrightarrow{V}_{circ}$ terms shown in Equation **??**.

where the plane defined by implicit surface function α_1 is at angle δ and plane α_2 is at constant height of $Z = 1$ shown in Equations 25 and 26 respectively.

$$\alpha_1 = cos(\delta)x + sin(\delta)y \tag{25}$$

$$\alpha_2 = z \tag{26}$$

The gradient ∇ of the potential function V is shown in Equation 27.

$$\nabla V = -\frac{1}{2(\sqrt{\cos^2(\delta)x^2 + 2\cos(\delta)\sin(\delta)xy + \sin^2(\delta)y^2})} \begin{bmatrix} 2x\cos^2(\delta) + 2\cos(\delta)\sin(\delta)y \\ 2y\sin^2(\delta) + 2\cos(\delta)\sin(\delta)x \\ 2 \end{bmatrix} \tag{27}$$

Circulation is calculated by the cross product of the surface function gradients, shown in Equation **??** and 28.

$$\overrightarrow{V}_{circ} = \begin{bmatrix} sin(\theta) \\ -cos(\theta) \\ 0 \end{bmatrix} \tag{28}$$

Guidance for a path at angle $\delta = 0$ and equal parts circulation and convergence weights $G = H = 1$ is shown in Figure 6 below.

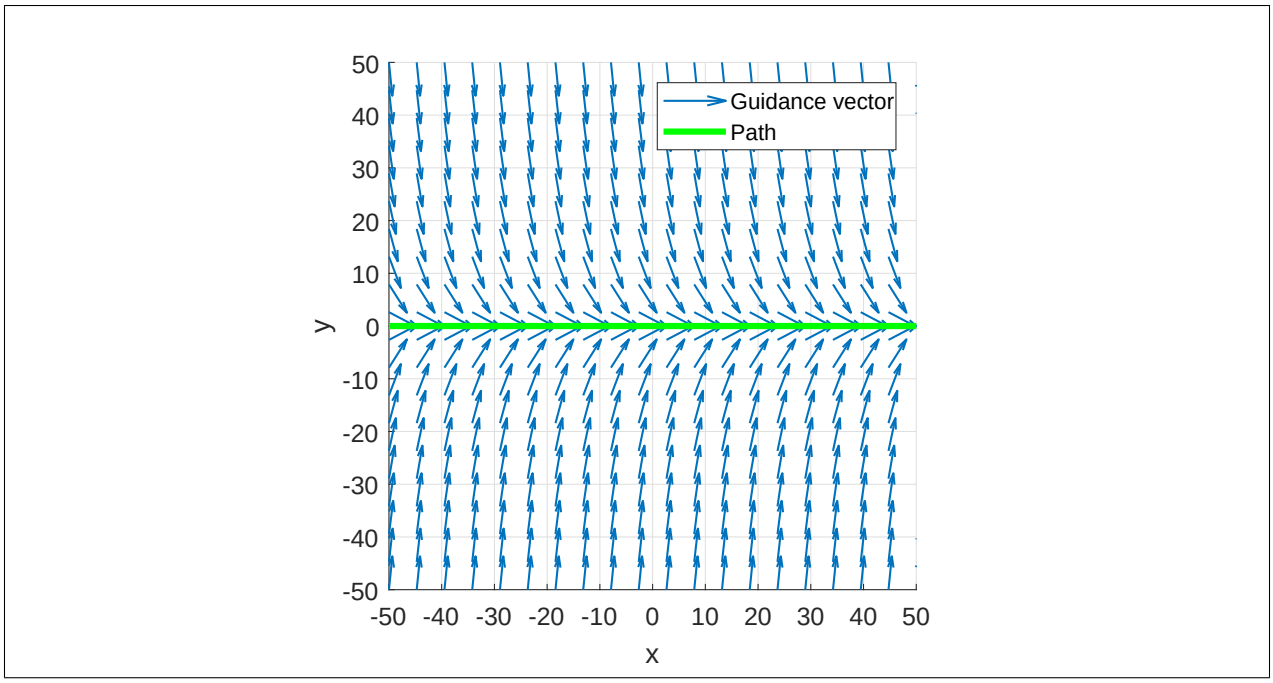

Fig. 6

B. Avoidance

Constructing a repulsive vector field for avoidance using the GVF method starts with constructing a vector field that converges and circulates a circular path. A GVF that converges and circulates a circular path is constructed with the implicit functions of a cylinder of radius r centered at (x_c, y_c) and a level plane of constant height Z, shown in Equations 29 and 30 below.

$$\alpha_1 = (x - x_c)^2 + (y - y_c)^2 - r^2 \tag{29}$$

$$\alpha_2 = z \tag{30}$$

Convergence is determined by the gradient of the potential function 27, which when simplified evaluates to

$$\overrightarrow{V}_{conv} = A\overrightarrow{B} \tag{31}$$

where

$$A = \frac{-1}{\sqrt{\bar{x}^4 + \bar{y}^4 + 2\bar{x}^2\bar{y}^2 - 2r^2\bar{x}^2 - 2r^2\bar{y}^2 + r^2 + z^2}} \tag{32}$$

and

$$\overrightarrow{B} = \begin{bmatrix} 2\bar{x}^3 + 2\bar{x}\bar{y}^2 - 2r^2\bar{x} \\ 2\bar{y}^3 + 2\bar{x}^2\bar{y} - 2r^2\bar{y} \\ z \end{bmatrix} \tag{33}$$

.

$$\bar{x} = x - x_c \tag{34}$$

$$\bar{y} = y - y_c \tag{35}$$

Circulation is calculated from the cross product of each implicit surface functions gradient, which simplifies to

$$\overrightarrow{V}_{circ} = \begin{bmatrix} 2(y - y_c) \\ -2(x - x_c) \\ 0 \end{bmatrix} \tag{36}$$

Guidance for avoiding a circular path with a large radius can be produced by setting the convergence weight $G = -1$ and circulation weight $H = 0$, shown in Figure 7. Note that the vectors are normalized prior to applying decay to ensure the vector field strength is bounded.

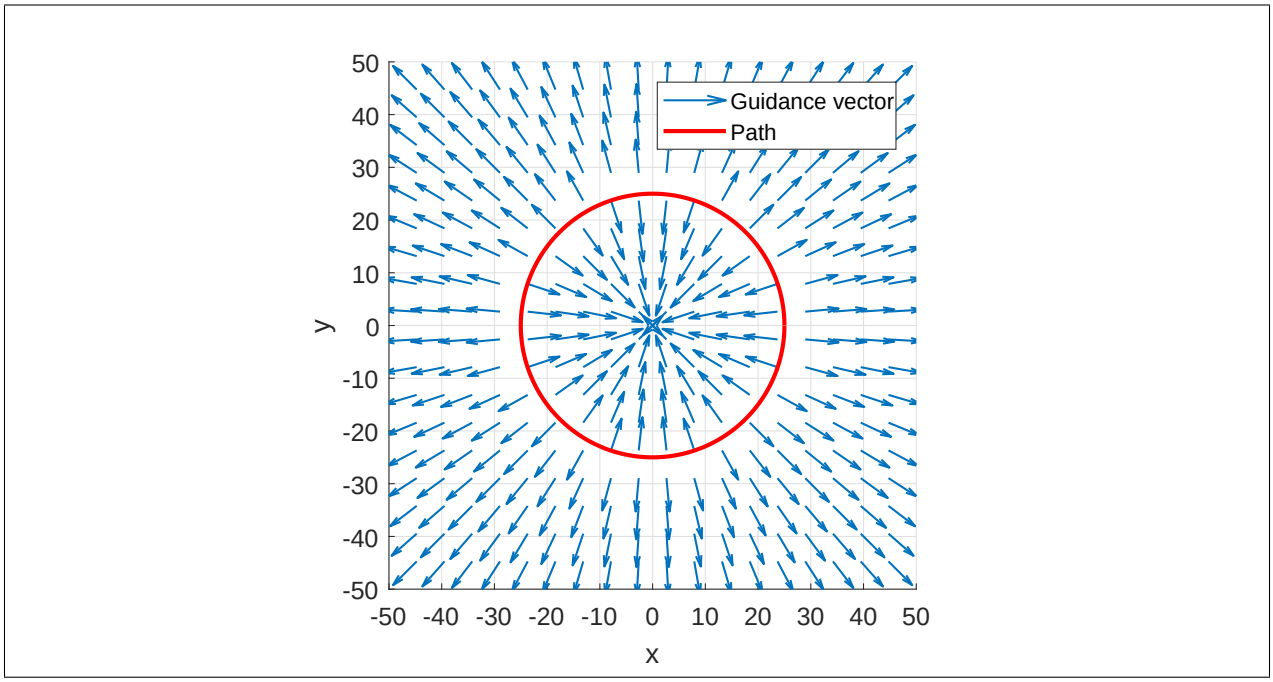

Fig. 7

Note that inside of the path, vectors point towards the center of the circle which may produce a trap situation if the UAV ends up inside the radius. To prevent a trap situation inside of the circular path, the radius of the path can be reduced, as shown in Figure 8 where $r = 0.01$.

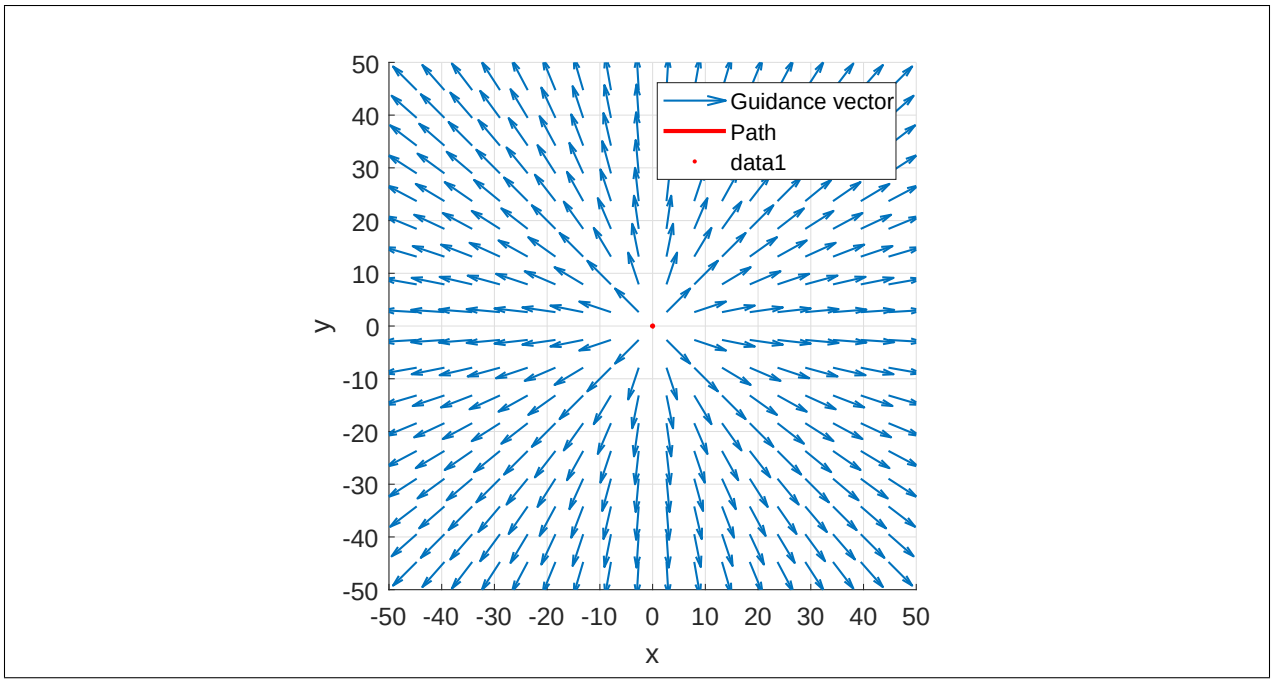

Fig. 8

To limit the influence of the repulsive field to a radius R, a decay function is applied prior to summing with the path following guidance. The decay strength P is determined in 37, where d is the euclidean distance, or range, between the UAV and the center of the obstacle, shown in Equation 38. At a distance $d > R$ the decay strength P is effectively zero, having virtual no influence on the total guidance. At a distance $d \leq R$, the field strength is bounded between $[0, 2]$.

$$P = -\tanh\left(\frac{2\pi d}{R} - \pi\right) + 1 \tag{37}$$

$$d = \sqrt{\bar{x}^2 + \bar{y}^2} \tag{38}$$

Applying the decay function with a decay edge radius $R = 35$ to the GVF shown in figure 8, results in the field shown in Figure 9.

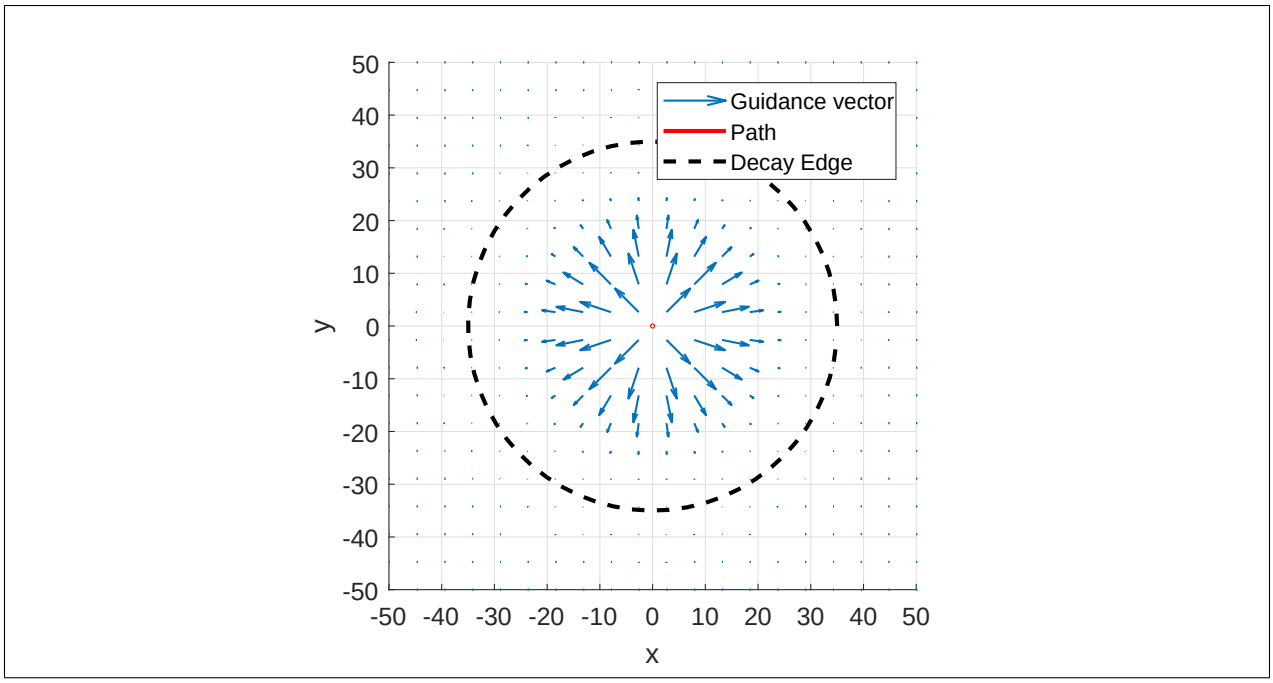

Fig. 9

Summing together the path following field with an obstacle centered on the path results in the guidance $\vec{V}_G$ shown in Figure 10.

$$\vec{V}_g = \vec{V}_{path} + P\vec{V}_{obst} \tag{39}$$

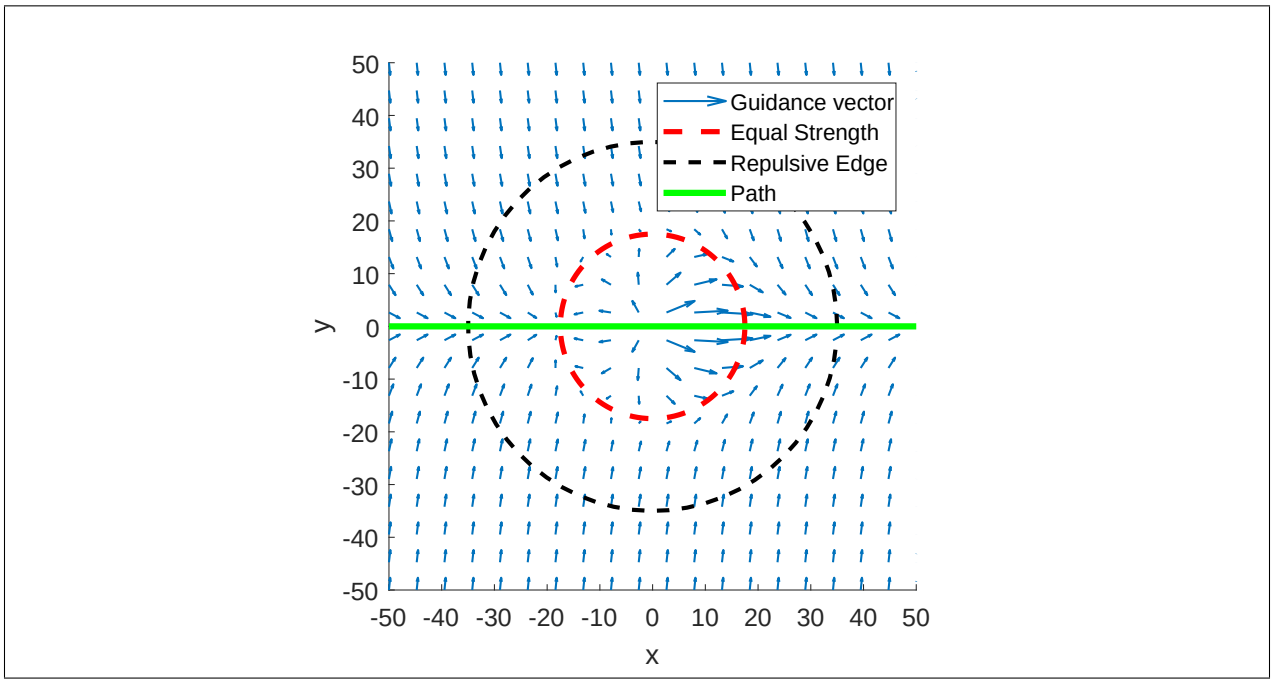

Fig. 10

C. Singularity Detection

$$||\overrightarrow{V}_g|| = 0 \tag{40}$$

Summing GVFs together may lead to small regions where the vector magnitude is near or equal to zero. Singularities are expected to exist where two summed fields have equal strength. The location of the singularities can be found by determining where the magnitude of the resulting guidance is equal to zero.

Plotting the magnitude of the summed field near the obstacle shows a well that descends into several local minimums called singularities, shown in Figure 11.

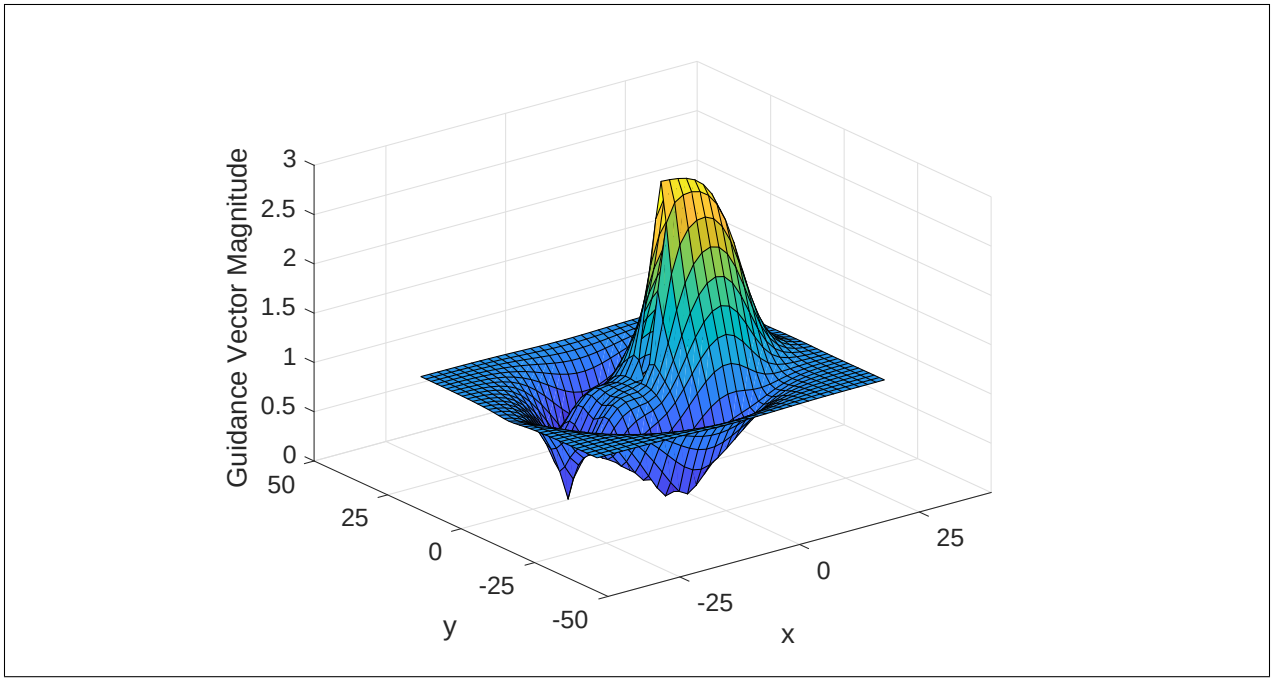

Fig. 11

Multiple singularities or near zero guidance regions may exist, so several initial conditions must be evaluated to increase the probability of detection. With the path and obstacle field shown in 10, several initial conditions evenly spaced were evaluated both inside and outside of the equal strength circle. Note how only points left of the obstacle were evaluated since this region is where attractive and repulsive vectors oppose each other, therefore it is where singularities are expected. Both inside and outside initial conditions determine the location of the singularities.

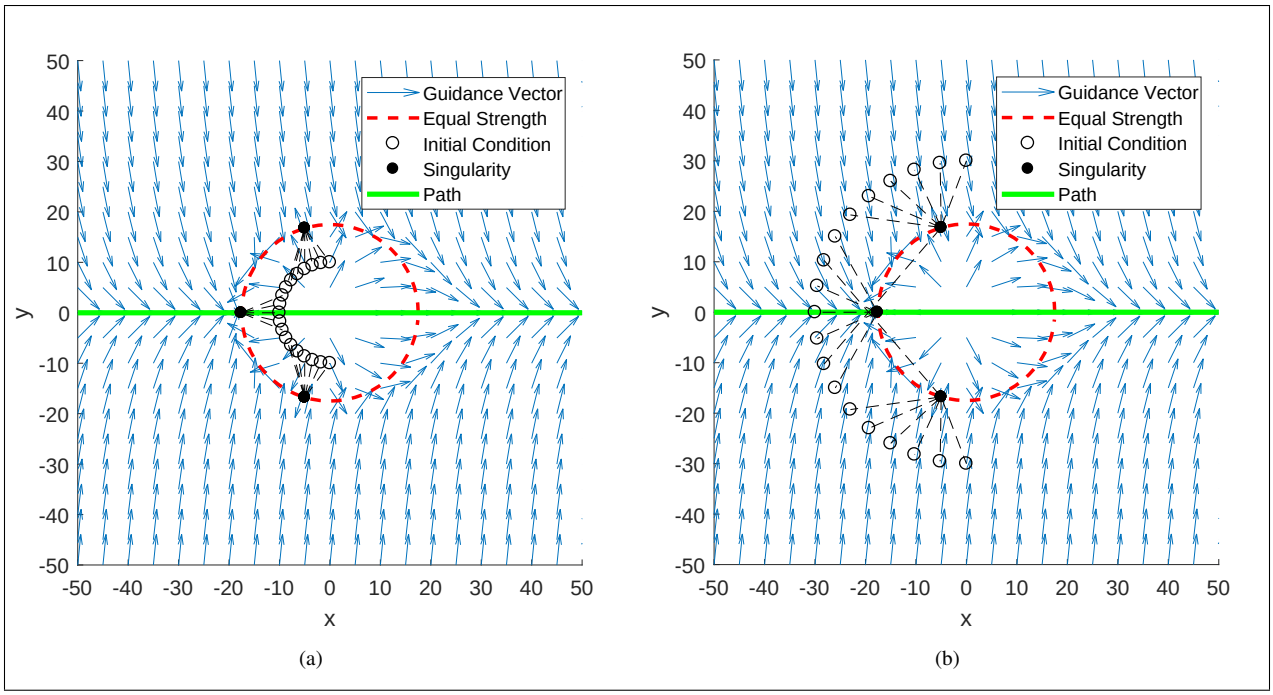

Fig. 12 GVF converging and circulating circular path

D. Flight Envelope

Evaluating a large number of initial conditions to improve the probability of finding singularities may be computationally expensive and may also find singularities the UAV may not encounter. Selecting a reduced set of initial conditions and to determine if the singularities exist where the UAV may fly, a flight envelope is determined for some time horizon t_h. Consider the UAV depicted in Figure 13 with a turn rate $\dot{\theta}$ and fixed speed u.

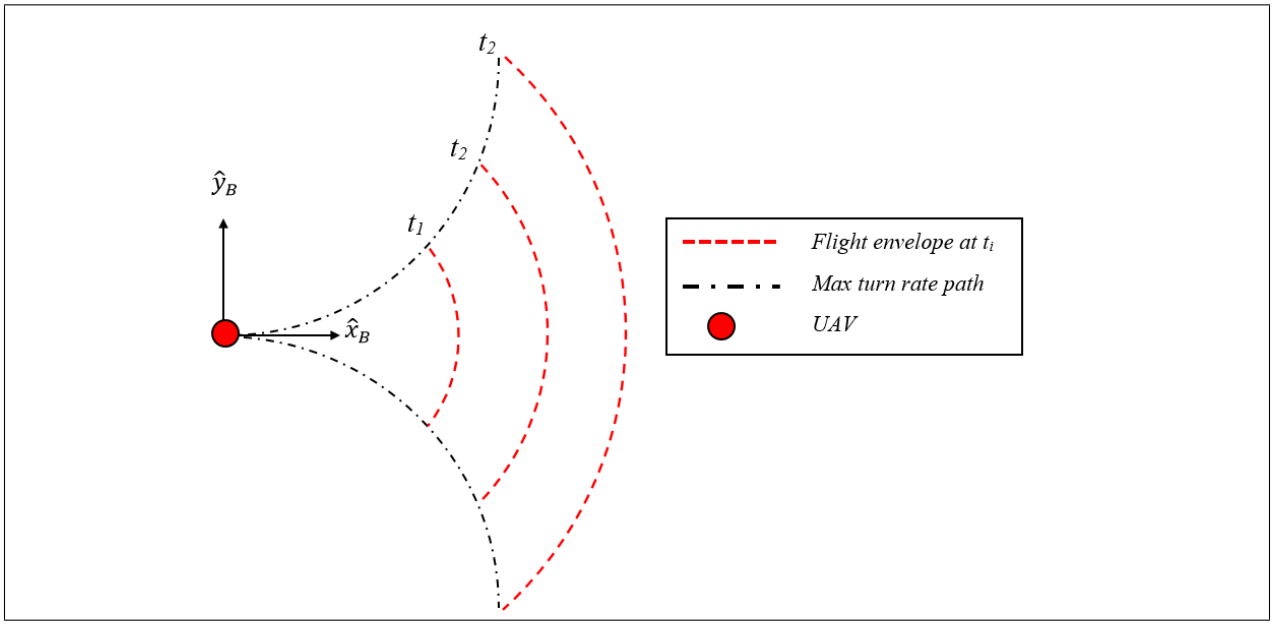

Fig. 13

The flight envelope, or positions the UAV, at time t_i with respect to the body frame is calculated in Equations 41 and 42

$$q_x = \frac{u}{\dot{\theta}} \sin(t_h \dot{\theta}) \tag{41}$$

$$q_y = \frac{u}{\dot{\theta}} \left(1 - \cos(t_h \dot{\theta})\right) \tag{42}$$

It is convenient to represent points on the flight envelope in the global inertial frame. The flight envelope points (q_x, q_y) can be expressed in vector form by finding the angle ϕ with respect to the body frame $\hat{x}_b$ axis and the vector magnitude q shown in equations 43 and 44 respectively.

$$\phi = \tan^{-1}\left(\frac{q_y}{q_x}\right) \tag{43}$$

$$q = \sqrt{q_x^2 + q_y^2} \tag{44}$$

$$\overrightarrow{Q_b} = \begin{bmatrix} q\cos\phi \\ q\sin\phi \\ 0 \end{bmatrix} \tag{45}$$

To express the flight envelope in the global inertial frame, the position vector of the UAV $\overrightarrow{P}_0$ and θ are applied with a rotation matrix R, shown in Equations 48, 46, and 47 below.

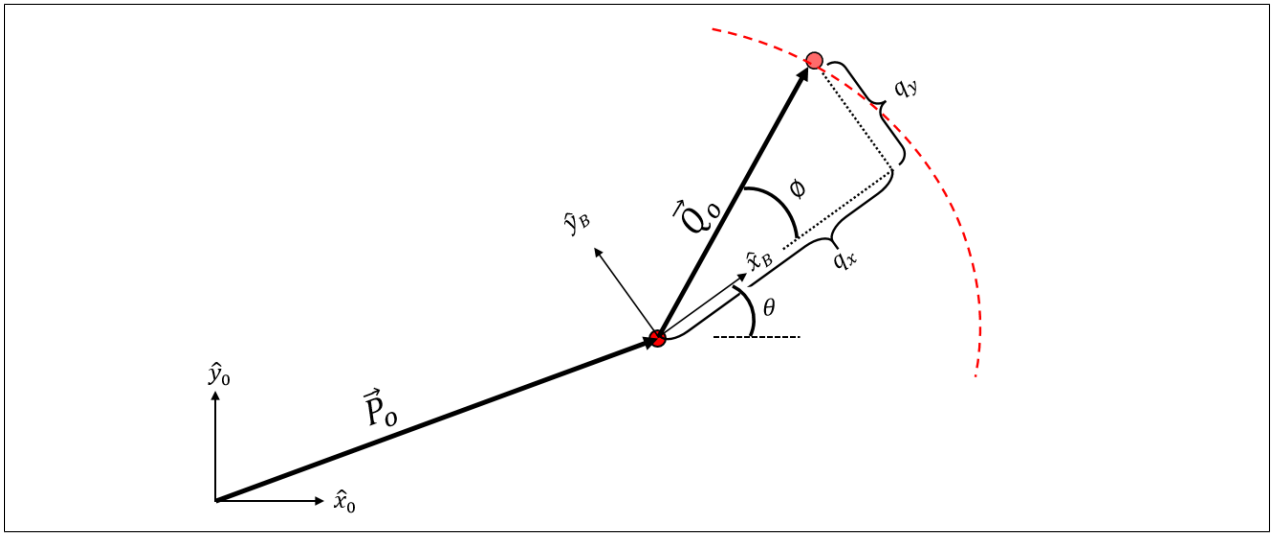

Fig. 14

$$\overrightarrow{P}_0 = \begin{bmatrix} x & y & 0 \end{bmatrix}^T \tag{46}$$

$$R = \begin{bmatrix} \cos(\theta) & -\sin(\theta) & 0 \\ \sin(\theta) & \cos(\theta) & 0 \\ 0 & 0 & 1 \end{bmatrix} \tag{47}$$

$$\overrightarrow{Q}_0 = \overrightarrow{P}_0 + R\overrightarrow{Q_b} \tag{48}$$

Initial conditions placed on the flight envelope will follow the magnitude gradient of the GVF guidance and locate any singularities it may encounter. When a singularity is found to exist inside or near a flight envelope the field can be modified to counteract it.

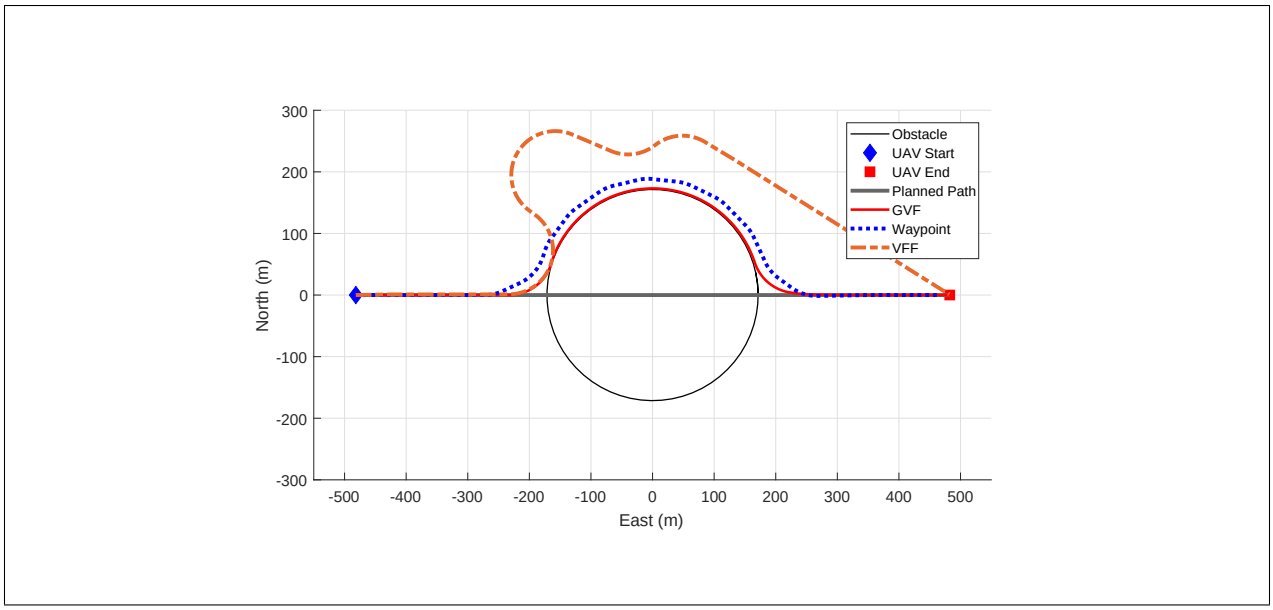

Fig. 15

V. Simulations

VI. Conclusion

Method	Cost (-)	RMS Error (m)
Waypoint	16.34	16.75
VFF	34.87	91.65
GVF	13.79	1.65

Appendix

Acknowledgments

References

[1] Ariyur, K. B., and Fregene, K. O., "Autonomous tracking of a ground vehicle by a UAV," *American Control Conference, 2008*, IEEE, 2008, pp. 669–671.

[2] Teuliere, C., Eck, L., and Marchand, E., "Chasing a moving target from a flying UAV," *Intelligent Robots and Systems (IROS), 2011 IEEE/RSJ International Conference on*, IEEE, 2011, pp. 4929–4934.

[3] Oh, H., Kim, S., Shin, H.-S., Tsourdos, A., and White, B., "Coordinated standoff tracking of groups of moving targets using multiple UAVs," *Control & Automation (MED), 2013 21st Mediterranean Conference on*, IEEE, 2013, pp. 969–977. URL `http://ieeexplore.ieee.org/abstract/document/6608839/`.

[4] Hyondong Oh, Seungkeun Kim, Hyo-sang Shin, and Tsourdos, A., "Coordinated standoff tracking of moving target groups using multiple UAVs," *IEEE Transactions on Aerospace and Electronic Systems*, Vol. 51, No. 2, 2015, pp. 1501–1514. doi:10.1109/TAES.2015.140044, URL `http://ieeexplore.ieee.org/document/7126199/`.

[5] Ulun, S., and Unel, M., "Coordinated motion of UGVs and a UAV," *Industrial Electronics Society, IECON 2013-39th Annual Conference of the IEEE*, IEEE, 2013, pp. 4079–4084. URL `http://ieeexplore.ieee.org/abstract/document/6699789/`.

[6] Oliveira, T., Aguiar, A. P., and Encarnacao, P., "Moving Path Following for Unmanned Aerial Vehicles With Applications to Single and Multiple Target Tracking Problems," *IEEE Transactions on Robotics*, Vol. 32, No. 5, 2016, pp. 1062–1078. doi:10.1109/TRO.2016.2593044, URL http://ieeexplore.ieee.org/document/7553466/.

[7] Khatib, O., "Real-time obstacle avoidance for manipulators and mobile robots," *The international journal of robotics research*, Vol. 5, No. 1, 1986, pp. 90–98. URL http://journals.sagepub.com/doi/abs/10.1177/027836498600500106.

[8] Rimon, E., "Exact Robot Navigation Using Artificial Potential Functions.pdf," , 1992.

[9] Borenstein, J., and Koren, Y., "Real-time obstacle avoidance for fast mobile robots in cluttered environments," *Robotics and Automation, 1990. Proceedings., 1990 IEEE International Conference on*, IEEE, 1990, pp. 572–577. URL http://ieeexplore.ieee.org/abstract/document/126042/.

[10] Borenstein, J., and Koren, Y., "The vector field histogram-fast obstacle avoidance for mobile robots," *IEEE transactions on robotics and automation*, Vol. 7, No. 3, 1991, pp. 278–288. URL http://ieeexplore.ieee.org/abstract/document/88137/.

[11] Koren, Y., and Borenstein, J., "Potential Field Methods and their inherent limitions for morbile robot navigation.pdf," , 1991. URL http://ieeexplore.ieee.org/document/131810/.

[12] Liu, Y., and Zhao, Y., "A virtual-waypoint based artificial potential field method for UAV path planning," *Guidance, Navigation and Control Conference (CGNCC), 2016 IEEE Chinese*, IEEE, 2016, pp. 949–953. URL http://ieeexplore.ieee.org/abstract/document/7828913/.

[13] Kim, D. H., "Escaping route method for a trap situation in local path planning," *International Journal of Control, Automation and Systems*, Vol. 7, No. 3, 2009, pp. 495–500. doi:10.1007/s12555-009-0320-7, URL http://link.springer.com/10.1007/s12555-009-0320-7.

[14] Goerzen, C., Kong, Z., and Mettler, B., "A Survey of Motion Planning Algorithms from the Perspective of Autonomous UAV Guidance," *Journal of Intelligent and Robotic Systems*, Vol. 57, No. 1-4, 2010, pp. 65–100. doi:10.1007/s10846-009-9383-1, URL http://link.springer.com/10.1007/s10846-009-9383-1.

[15] Lei Tang, Songyi Dian, Gangxu Gu, Kunli Zhou, Suihe Wang, and Xinghuan Feng, "A novel potential field method for obstacle avoidance and path planning of mobile robot," IEEE, 2010, pp. 633–637. doi:10.1109/ICCSIT.2010.5565069, URL http://ieeexplore.ieee.org/document/5565069/.

[16] Li, G., Yamashita, A., Asama, H., and Tamura, Y., "An efficient improved artificial potential field based regression search method for robot path planning," IEEE, 2012, pp. 1227–1232. doi:10.1109/ICMA.2012.6283526, URL http://ieeexplore.ieee.org/document/6283526/.

[17] Sujit, P., Saripalli, S., and Sousa, J. B., "Unmanned Aerial Vehicle Path Following: A Survey and Analysis of Algorithms for Fixed-Wing Unmanned Aerial Vehicless," *IEEE Control Systems*, Vol. 34, No. 1, 2014, pp. 42–59. doi:10.1109/MCS.2013.2287568, URL http://ieeexplore.ieee.org/document/6712082/.

[18] Nelson, D. R., "Cooperative control of miniature air vehicles," 2005. URL http://scholarsarchive.byu.edu/etd/1095/.

[19] Nelson, D. R., Barber, D. B., McLain, T. W., and Beard, R. W., "Vector field path following for small unmanned air vehicles," *American Control Conference, 2006*, IEEE, 2006, pp. 7–pp. URL http://ieeexplore.ieee.org/abstract/document/1657648/.

[20] Nelson, D., Barber, D., McLain, T., and Beard, R., "Vector Field Path Following for Miniature Air Vehicles," *IEEE Transactions on Robotics*, Vol. 23, No. 3, 2007, pp. 519–529. doi:10.1109/TRO.2007.898976, URL http://ieeexplore.ieee.org/document/4252175/.

[21] Frew, E. W., "Cooperative standoff tracking of uncertain moving targets using active robot networks," *Robotics and Automation, 2007 IEEE International Conference on*, IEEE, 2007, pp. 3277–3282. URL http://ieeexplore.ieee.org/abstract/document/4209596/.

[22] Miao, Z., Thakur, D., Erwin, R. S., Pierre, J., Wang, Y., and Fierro, R., "Orthogonal vector field-based control for a multi-robot system circumnavigating a moving target in 3D," *Decision and Control (CDC), 2016 IEEE 55th Conference on*, IEEE, 2016, pp. 6004–6009. URL http://ieeexplore.ieee.org/abstract/document/7799191/.

[23] Griffiths, S., "Vector Field Approach for Curved Path Following for Miniature Aerial Vehicles," American Institute of Aeronautics and Astronautics, 2006. doi:10.2514/6.2006-6467, URL http://arc.aiaa.org/doi/10.2514/6.2006-6467.

[24] Goncalves, V. M., Pimenta, L. C. A., Maia, C. A., and Pereira, G. A. S., "Artificial vector fields for robot convergence and circulation of time-varying curves in n-dimensional spaces," IEEE, 2009, pp. 2012–2017. doi:10.1109/ACC.2009.5160350, URL http://ieeexplore.ieee.org/document/5160350/.

[25] Gonçalves, V. M., Pimenta, L. C., Maia, C. A., Pereira, G. A., Dutra, B. C., Michael, N., Fink, J., and Kumar, V., "Circulation of curves using vector fields: actual robot experiments in 2D and 3D workspaces," *Robotics and Automation (ICRA), 2010 IEEE International Conference on*, IEEE, 2010, pp. 1136–1141.

[26] Gonçalves, V. M., Pimenta, L. C., Maia, C. A., Dutra, B. C., and Pereira, G. A., "Vector fields for robot navigation along time-varying curves in $ n $-dimensions," *IEEE Transactions on Robotics*, Vol. 26, No. 4, 2010, pp. 647–659. URL http://ieeexplore.ieee.org/abstract/document/5504176/.

[27] Gerlach, A. R., *Autonomous Path-Following by Approximate Inverse Dynamics and Vector Field Prediction*, University of Cincinnati, 2014. URL http://search.proquest.com/openview/432d738d856bf0a9b46acea1b1eee08f/1?pq-origsite=gscholar&cbl=18750&diss=y.

[28] Jung, W., Lim, S., Lee, D., and Bang, H., "Unmanned Aircraft Vector Field Path Following with Arrival Angle Control," *Journal of Intelligent & Robotic Systems*, Vol. 84, No. 1-4, 2016, pp. 311–325. doi:10.1007/s10846-016-0332-5, URL http://link.springer.com/10.1007/s10846-016-0332-5.

[29] Panagou, D., "Motion planning and collision avoidance using navigation vector fields," *Robotics and Automation (ICRA), 2014 IEEE International Conference on*, IEEE, 2014, pp. 2513–2518. URL http://ieeexplore.ieee.org/abstract/document/6907210/.